

Supporting Information

Characterization of SMPS

Table S1. Textual properties of MPSs and SMPSs

Samples	SSA ^(a)	TPV ^(b)	D _{pore}			D ₍₁₀₀₎ ^(f)	D _{ptp} ^(g)	D _{wall} ^(h)
	BET		BJH ^(c)	GCMC ^(d)	H-K ^(e)			
	m ² /g	cm ³ /g	nm	nm	nm	nm	nm	nm
C18MPS	1361	0.96	3.00	3.27	3.36	3.18	3.67	0.40
C16MPS	1452	0.79	2.70	2.82	2.86	2.88	3.32	0.50
C14MPS	1234	0.60	-	2.26	2.4	2.94	3.39	1.13
C12SMPS	1056	0.53	-	1.82	2.00	2.61	3.01	1.19
C10SMPS	916	0.45	-	1.58	1.60	2.36	2.72	1.14
C8SMPS	810	0.41	-	1.28	-	2.47	2.85	1.57
C6SMPS	632	0.32	-	1.12	-	2.36	2.73	1.61
C4SMPS	586	0.29	-	0.92	-	2.50	2.89	1.97
C8VSMPS ⁽ⁱ⁾	519	0.25	-	0.99	-	2.05	2.37	1.38
C6VSMPS ⁽ⁱ⁾	582	0.25	-	0.82	-	1.73	2.00	1.18
C4VSMPS ⁽ⁱ⁾	355	0.16	-	0.77	-	1.71	1.98	1.21

(a) Specific surface area calculated from BET method. (b) Total pore volume. (c), (d) (e) Calculated average pore diameters using BJH, GCMC, and H-K analysis. (f) The peak position of (100) diffraction in SAXRD pattern. (g) The pore-to-pore distance calculated from D₁₀₀. (h) The wall thickness calculated from GCMC average pore diameters and pore-to pore distances. (i) "V" represents the use of TEVS.

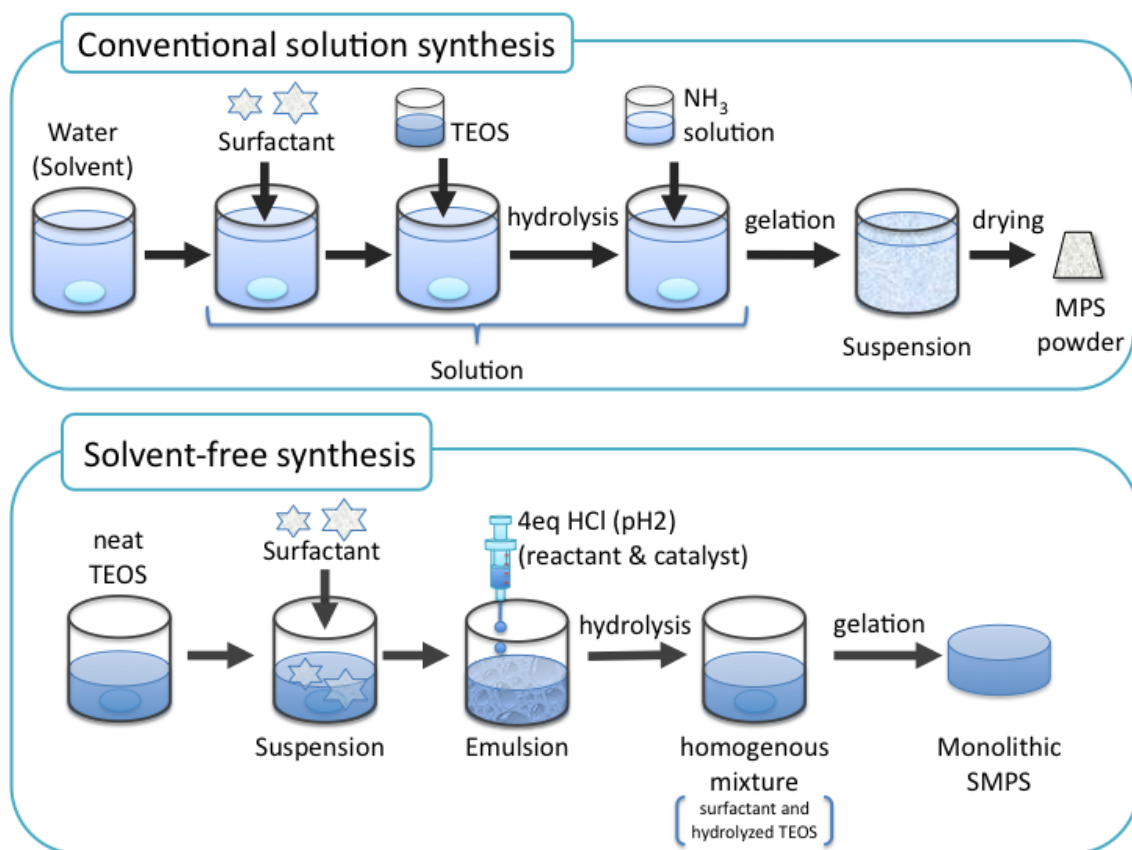


Figure S1. Reaction scheme of conventional MPS synthesis and present solvent-free SMPS syntheses.

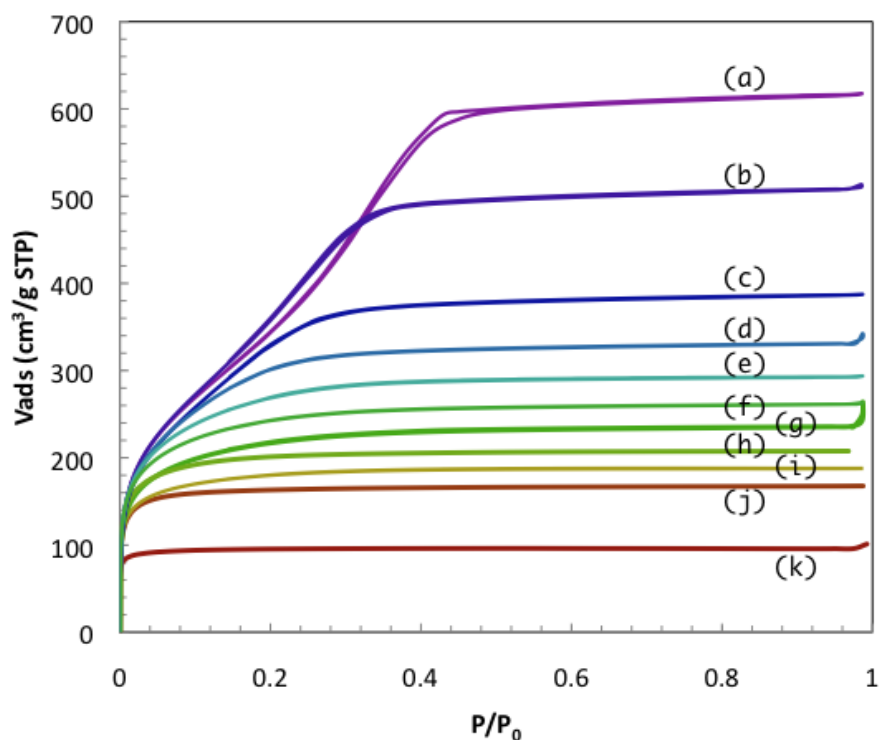


Figure S2. Nitrogen adsorption-desorption isotherms of porous silicas synthesized with various surfactants. (a) C18, (b) C16, (c) C14, (d) C12, (e) C10, (f) C8, (g) C6, (h) C6V, (i) C8V, (j) C4, (k) C4V. ("V" represents the use of TEVS)

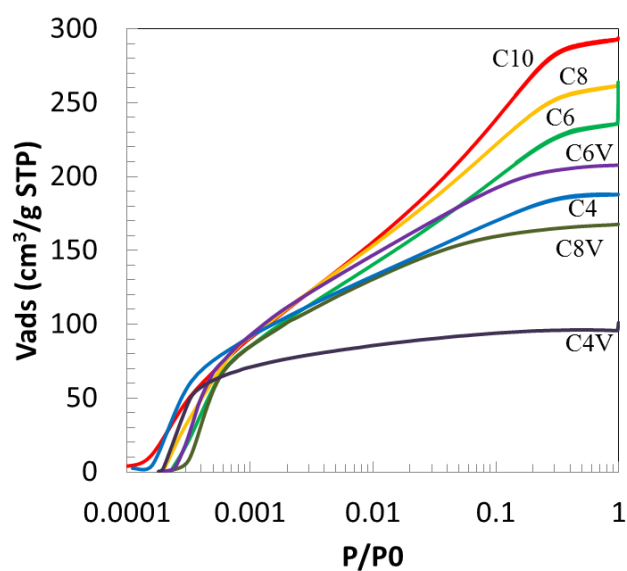


Figure S3. Logarithm scaled nitrogen adsorption-desorption isotherms of SMPSs.

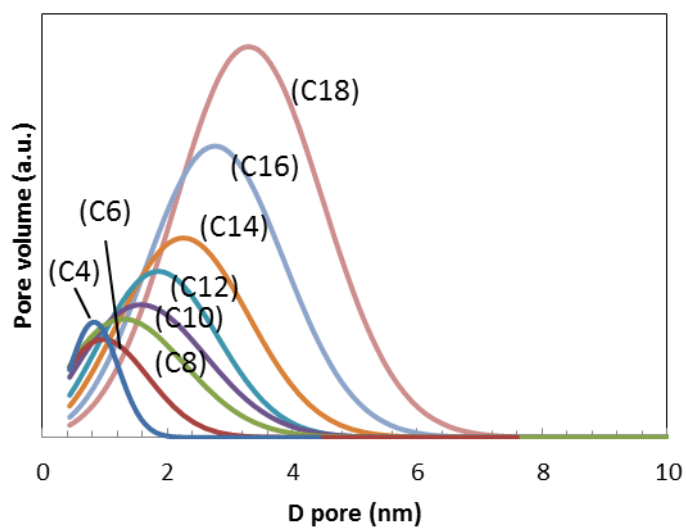


Figure S4. The GCMC pore size distribution of C18MPS (right) to C4SMPS (left).

The present GCMC analyses gave good results with average pore size estimation, however, this method over estimates about size distribution compared to BJH analyses.

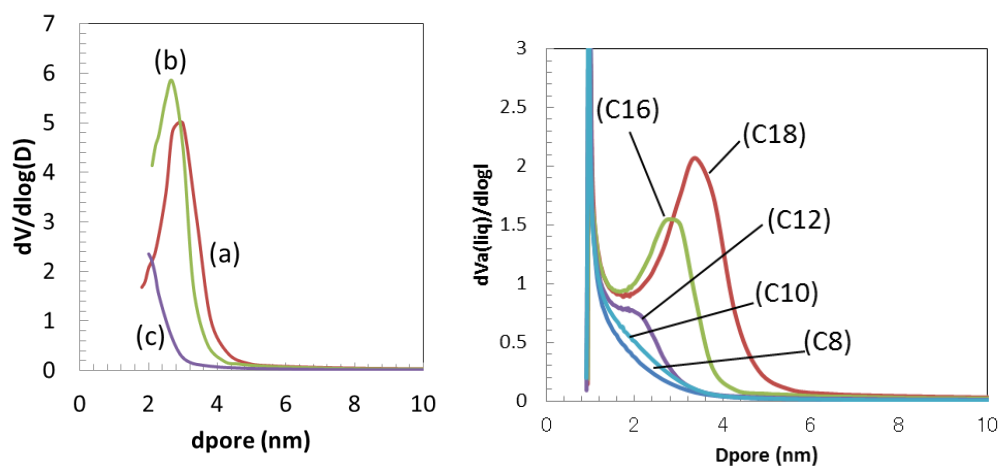


Figure S5. The pore size distribution by using BJH method (left) (a) C18MPS, C16MPS, and C12MPS and H-K method (right). Each method fits well only in the range with pore diameter >2 nm (BJH) and >1.5 nm (H-K), respectively.

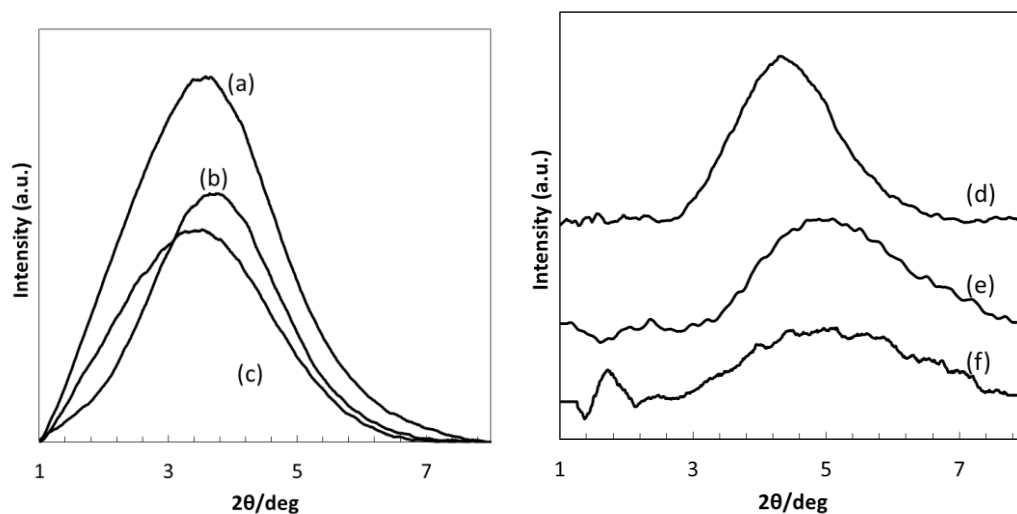


Figure S6. Small angle X-ray diffraction pattern of SMPSs and SNPSs (a) C8-SMPS, (b) C6-SMPS, (c) C4-SMPS, (d) C8V-SMPS, (e) C6V-SMPS, (f) C4V-SMPS, respectively.

A broad peak around 3 to 6 degree indicates a formation of wormhole like pore structure of the present porous silica.

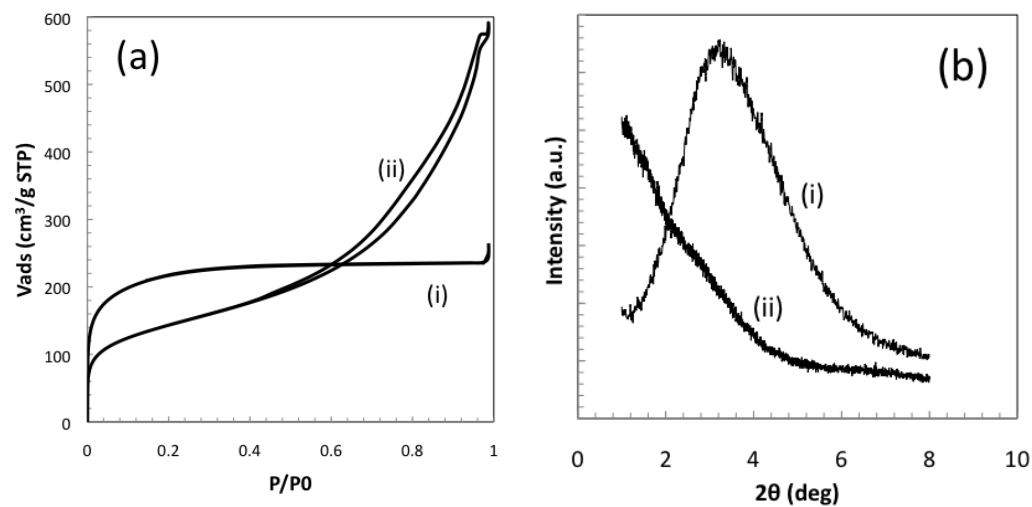


Figure S7. (a) Nitrogen adsorption-desorption isotherms and (b) XRD patterns of (i) C6-SMPS, and (ii) the product obtained via a solution reaction by using C₆TABr. The type IV isotherm (classification of IUPAC) in the nitrogen adsorption and absence of a peak in the XRD pattern indicate a production of amorphous silica (or silica nano-particle) in the case of solution reaction.

Characterization of WO₃

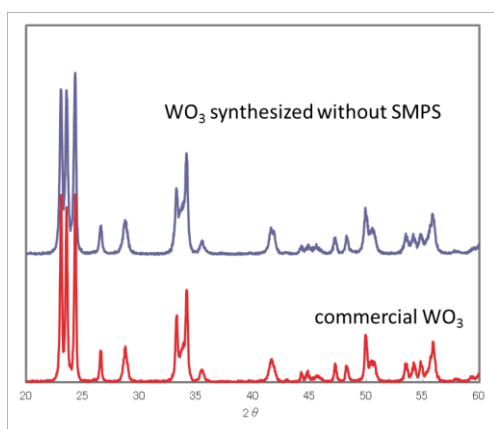


Figure S8. Powder X-ray diffraction patterns of WO₃ particles prepared without a silica matrix and commercial WO₃ powder.

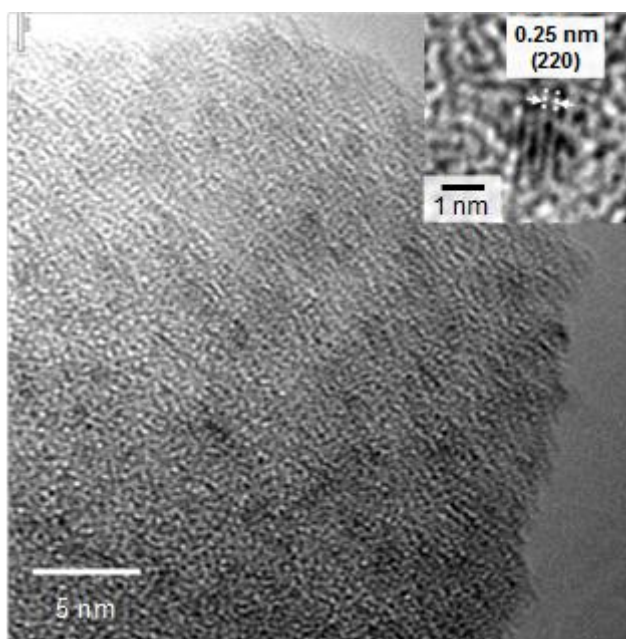


Figure S9. TEM images of C4V-W. The inset image shows the lattice fringe of monoclinic WO₃ assigned for the (220) plane.

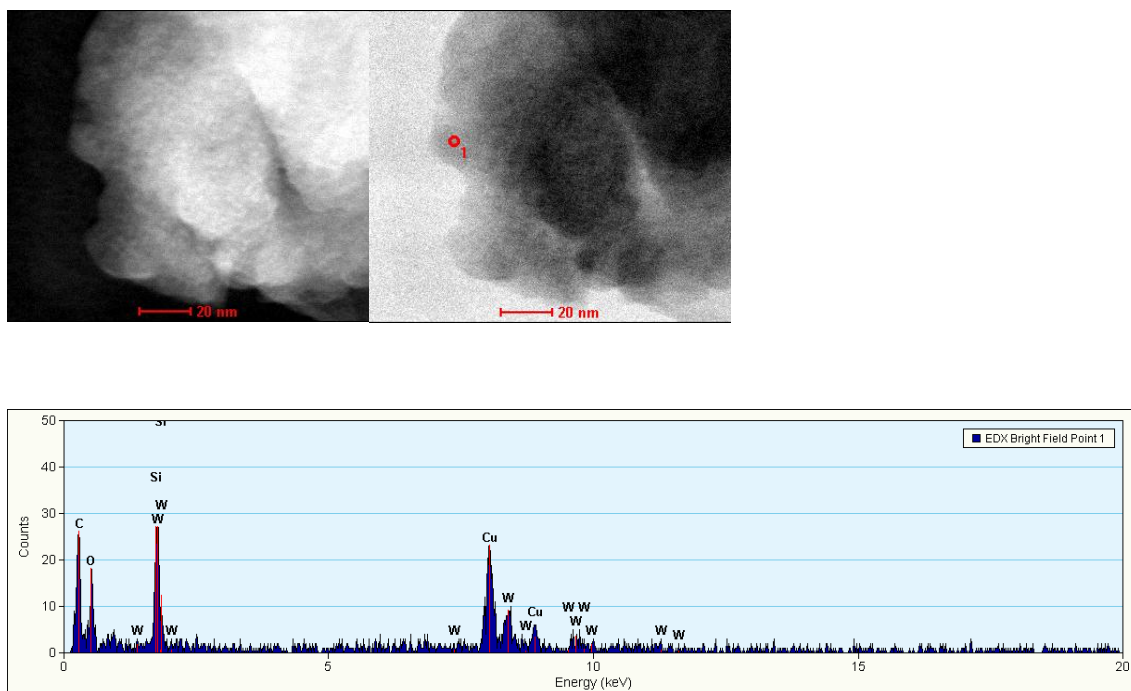


Figure S10. (Top) HAADF-STEM (High-Angle Annular Dark Field Scanning TEM) images of C6-W sample. (left: dark field), (right: bright field). (Bottom) EDS spectrum of the C6-W sample. (The measured area is displayed with red circle in the bright field TEM image. The peak assigned for Cu is from Cu grid.)

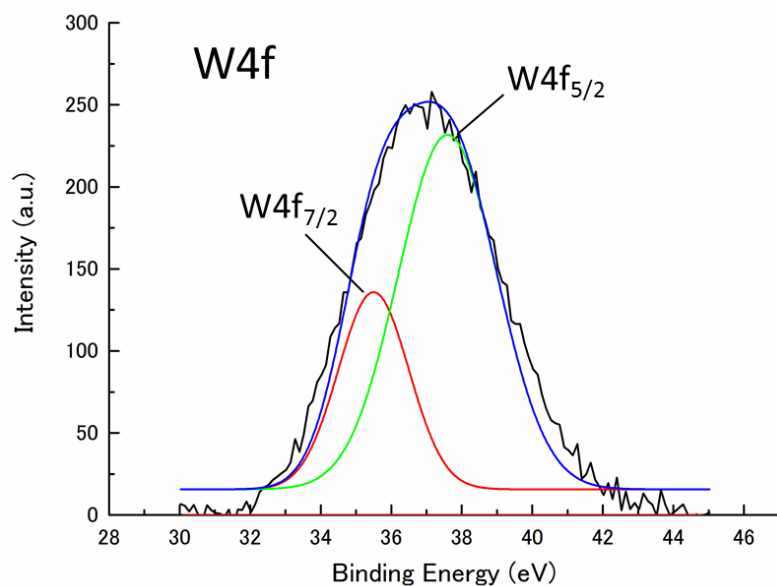


Figure S11. XPS spectrum for W4f core level of the C6-W sample. (Black) measured, (Blue) fitted curve, and Gaussian deconvoluted curve for W4f_{7/2} (35.7 eV, Red) and W4f_{5/2} (37.8 eV, Green) of WO₃, respectively.

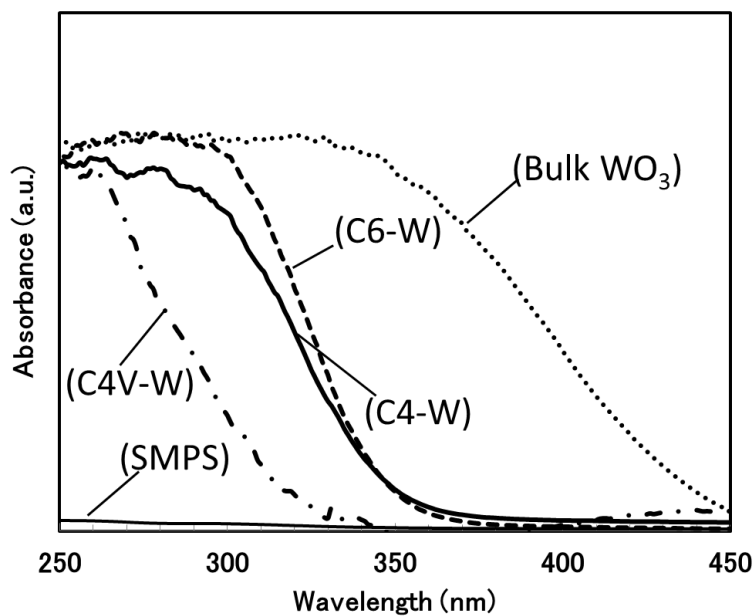


Figure S12. DR-UV-Vis spectrum for WO₃-QDs and SMPS. SMPS is totally transparent in whole UV-Vis region. Thus, contribution from silica to the optical band-gap determination is negligible.

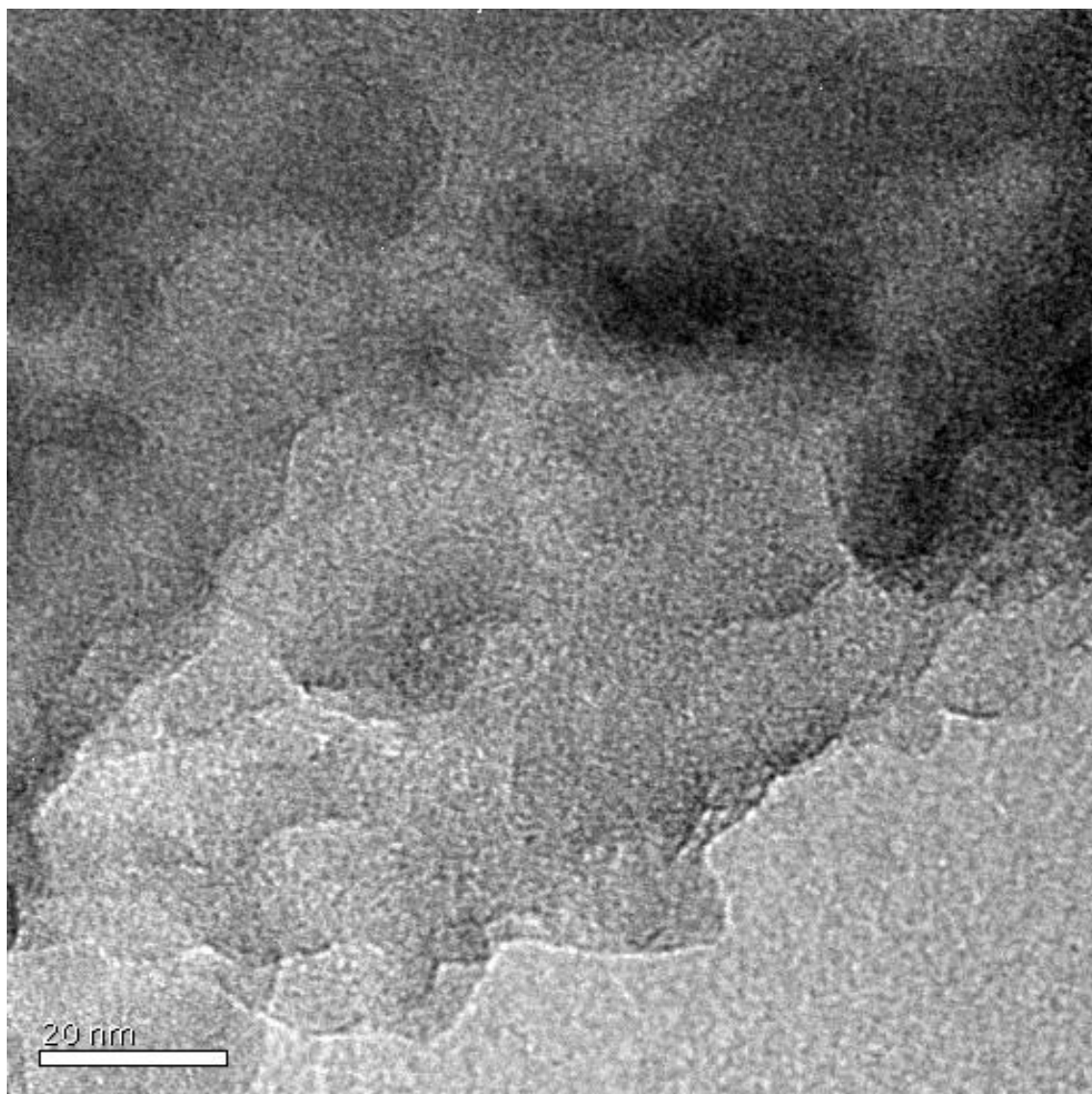


Figure S13. TEM images of C6SMPS.

Quantum size effect

Calculation of E_g by using effective mass approximation (EMA) theory

The relationship between E_g and the particle radius (R) of semiconductor is described by Brus as follow. [1]

$$E_g = E_{g0} + \frac{\hbar^2 \pi^2}{2R^2} \frac{1}{\mu} - \frac{1.8e^2}{\epsilon R} + \text{smaller terms} \quad (\text{Eq. 1})$$

Here, μ is a reduced mass of electron and hole. For a small gap semiconductor, the contribution of the Coulomb term (the 3rd term: which shift E^* to lower energy) is far smaller than that of the quantum localization term (the 2nd term: which shift E^* to higher energy). Thus, the cancellation from Coulomb term should not be important. [1]

The value μ can be written by using effective mass of electron (m_e^*) and hole (m_h^*) as follow.

$$\frac{1}{\mu} = \left(\frac{1}{m_e^*} + \frac{1}{m_h^*} \right) \quad (\text{Eq. 2})$$

Several m_e^* value of WO_3 were reported in the literature (i.e. $0.5m_0$, $0.7m_0$, and $1.8m_0$) [2, 3, 4], and none was reported for m_h^* . Therefore, we calculated μ value from experimental data reported in our previous study (1.4 nm WO_3 dot ($E_g = 3.05$ eV)). [5] By using this data μ was calculated as $1.69m_0$ which is close to the previously reported value of TiO_2 ($1.63m_0$). [6]

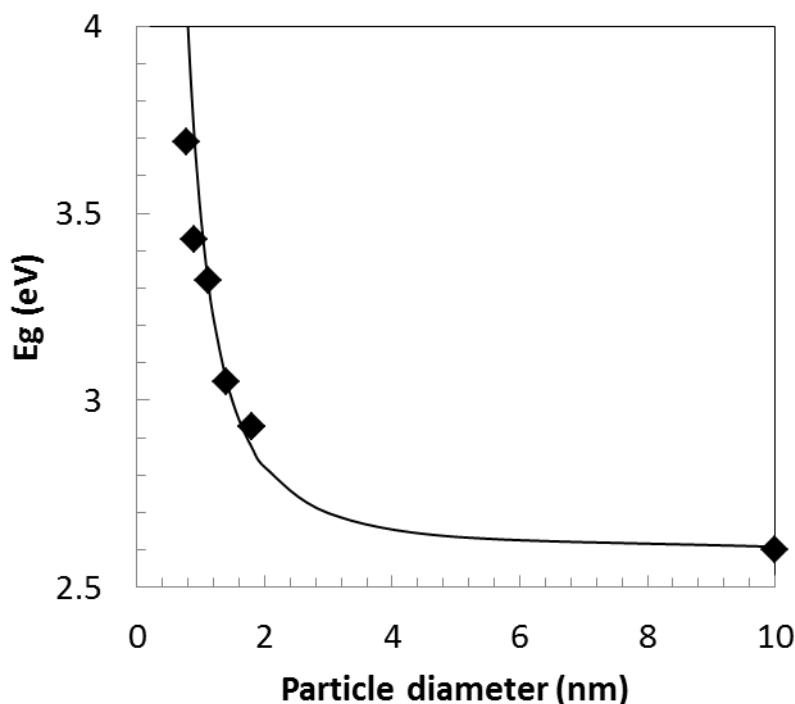


Figure S13 Correlation between E_g and the particle diameter of WO_3 -QDs ($\mu = 1.69 m_0$) (Solid line: calculated value by using EMA theory, Plots: experimental data from our study)

The relationship between E_g and particle size by using $\mu = 1.69 m_0$, was shown in Figure S13 (Figure 3b in the main text) with our experimental value. The experimental and theoretical value is well consistent in the nanometer region. However theoretical value overestimates a Q-size effect in sub-nanometer region. This trend is similar to the other semiconductor QDs, i.e CdSe etc. [7] We used this μ value for further calculations.

Calculation of E_{CB} and E_{VB} using EMA theory

We are now able to calculate the m^*_h by comparing several literature m^*_e value. If the value $m^*_e = 0.5m_0$ or $0.7m_0$ was used for the calculation, m^*_h becomes negative. This is not realistic. When we used a value $m^*_e = 1.8 m_0$ for the calculation, we obtained the value $m^*_h = 29 m_0$. We use this m^*_h value for the further calculation.

The relationship between quantum confinement energy ($E_{e/h}$) and a particle size of semiconductor is calculated by using following equation.

$$E_{e/h} = \frac{\hbar^2 \pi^2}{2m^*_{e/h} R^2} \quad (\text{Eq. 3})$$

The correlation between E_{CB} , E_{VB} and the particle diameter of WO_3 -QDs by using the value $m^*_e = 1.8 m_0$ and $m^*_h = 29 m_0$ were plotted in figure S14 (Figure 3c in the main text).

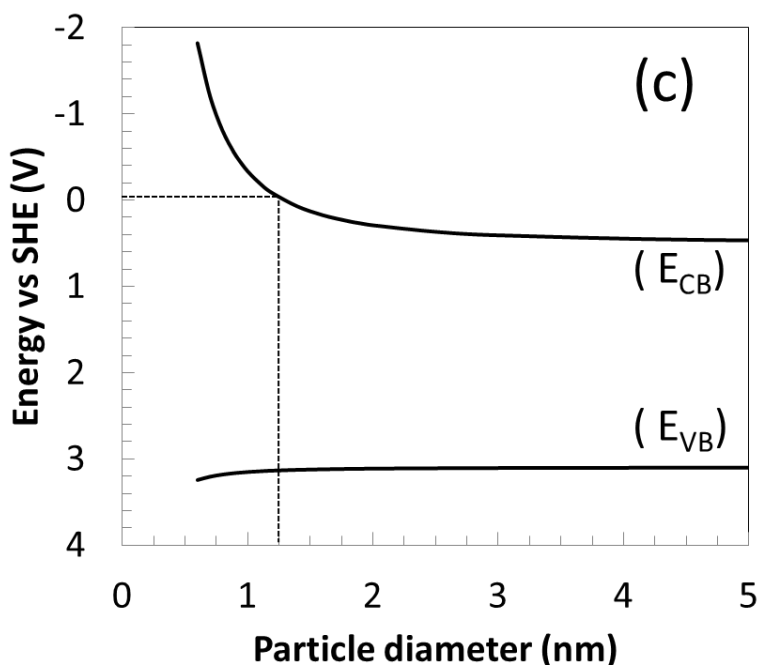


Figure S14. Correlation between E_{CB} , E_{VB} and the particle diameter of WO_3 -QDs.
($m^*_e = 1.8 m_0$, $m^*_h = 29 m_0$)

The E_{CB} shows a steep increase below 1 nm, while the shift of E_{VB} was smaller. These trends are also consistent to the case of CdSe etc. which has a smaller m^*_h than m^*_e . [7] Theoretically, when the particle diameter is smaller than 1.2 nm, the E_{CB} of WO_3 -QDs exceeds the single electron reduction potential of O_2 . The estimated E_{CB} calculated by EMA theory of C4-W was $-0.55 V_{SHE}$ (for $2R = 0.89$ nm). In the same manner, E_g was calculated as 3.72 eV. Thus the overestimation of Q-size effect in EMA theory in this size is estimated to be $\Delta E_g = 0.29$ eV. By taking into account this overestimation, the E_{CB} of C-4W sample is calculated as $-0.26 V_{SHE}$, which is higher than the reduction potential of O_2 . Therefore, it is reasonable to understand the experimental results that the photo reduction of O_2 take place with C4-W sample.

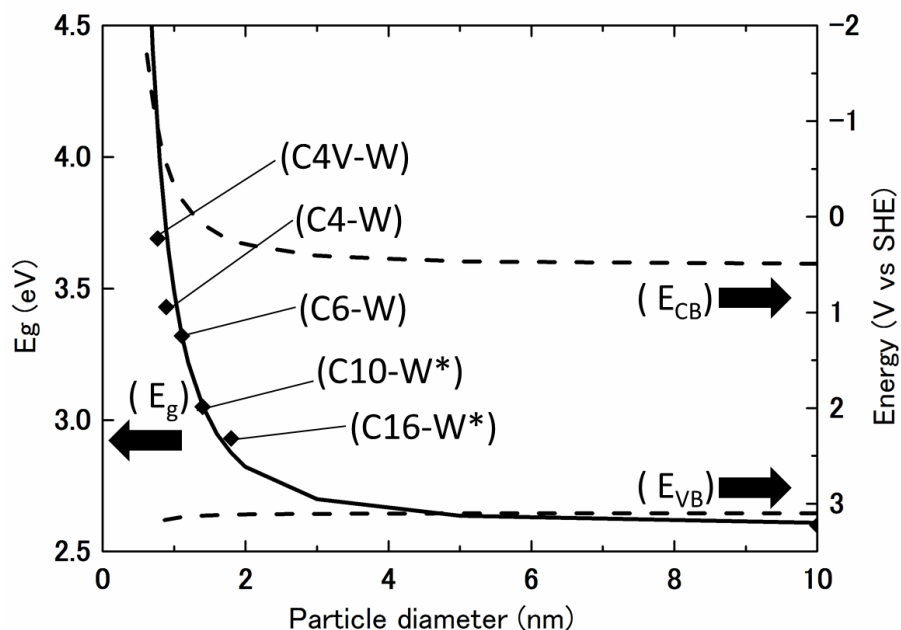


Figure S15. Correlation between, E_g , E_{CB} , E_{VB} and the particle diameter of WO_3 -QDs. Solid line: E_g (left axis), Dotted line: E_{CB} , E_{VB} (right axis). (Calculated by EMA theory; $m_e^* = 1.8 m_0$, $m_h^* = 29 m_0$) Plots: optical E_g and TEM average diameter (* Data from our previous study)

References

- [1] L. Brus, *J. Phys. Chem.* **1986**, *90*, 2555-2560.
- [2] J. Khalack, P. V. Ashrit, *Appl. Phys. Lett.*, **2006**, *89*, 211112.
- [3] B. L. Crowder, M. J. Sienko, *J. Chem. Phys.*, **1963**, *38*, 1567-1583.
- [4] H. Chen, N. Xu, S. Deng, J. Zhou, Z. Li, H. Ren, J. Chen, J. She, *J. Appl. Phys.*, **2007**, *101*, 114303-114305.
- [5] D. Tanaka, Y. Oaki, H. Imai, *Chem. Commun.* **2010**, *46*, 5286-5288.
- [6] N. Satoh, T. Nakashima, K. Kamikura, K. Yamamoto, *Nature Nanotech.* **2008**, *3*, 106-111.
- [7] (a) J. Jasieniak, M. Califano, S. E. Watkins, *ACS NANO*, **2011**, *5*, 5888-5902; (b) S. N. Inamdar, P. P. Ingole, S. K. Haram, *Chem. Phys. Chem.*, **2008**, *9*, 2574-2579; (c) L. Wang, A. Zunger, *Phys. Rev. B*, **1996**, *53*, 9579-9582.
- [8] M. T. Grenier, M. G. Helander, W. Tang, Z. Wang, J. Qiu, Z. Lu, *Nature Mater.*, **2012**, *11*, 76-81.

Experimental procedures

Materials

Tetraethylorthosilicate (TEOS), tetramethylorthosilicate (TMOS), triethoxyvinylsilane (TEVS), octadecyltrimethylammonium chloride ($C_{18}TACl$), hexadecyltrimethylammonium chloride ($C_{16}TACl$), tetradecyltrimethylammonium bromide ($C_{14}TABr$), dodecyltrimethylammonium bromide ($C_{12}TABr$), decyltrimethylammonium bromide ($C_{10}TABr$), octyltrimethylammonium bromide (C_8TABr), hexyltrimethylammonium bromide (C_6TABr), and dimethylpyrrolone-N-oxide (DMPO) were purchased from the Tokyo Kasei Kogyo Co. Butyltrimethylammonium chloride (C_4TACl) was purchased from AK Scientific, Inc. Hydrogen peroxide (H_2O_2), hydrochloric acid (HCl), and tungsten acid (H_2WO_4) were purchased from the Junsei Chemical Co. All the materials were used as purchased.

Solvent-free syntheses of supermicroporous silica

Long-chain surfactant in the amount of 7.5 mmol ($C_{18}TACl$ or $C_{16}TACl$ or $C_{14}TABr$ or $C_{12}TABr$ or $C_{10}TABr$) or short chain surfactant in the amount of 22.5 mmol (C_8TABr or C_6TABr or C_4TACl) was suspended in 37.5 mmol of tetraethylorthosilicate (TEOS) in a closed polypropylene vessel. For the pore size reduction using TEVS, 1.925 mmol (5 mol% versus TEOS) of TEVS was added to the mixture, and then 152 mmol (4 equivalents versus TEOS) of water, acidified to pH 2 using hydrochloric acid, was added to that suspension. The mole composition of TEOS/ H_2O / C_nTAX was set to 1.0 : 4.0 : 0.2-1.0. After stirring for 1 h, the suspension turned to a clear solution with the hydrolysis of TEOS. The solution was continuously stirred at room temperature for 1 day to several days or overnight at 333 K to complete gelation. The obtained transparent gel was dried at 333 K and calcined at 873 K for 3 h at a heating rate of 5 K/min to remove the templates. After calcination, colorless transparent supermicroporous silica was obtained.

Preparation of aqueous solution of peroxotungstic acid (WO₃ precursor solution)

A yellowish powder of 2.0 g of tungsten acid (H₂WO₄) was suspended in the mixture of 20 mL of H₂O and 20 mL of an H₂O₂ solution. The final concentration of peroxotungstic acid and H₂O₂ was fixed to 0.2 M and 20 M, respectively. The suspension was stirred overnight at R.T. to obtain a colorless clear solution of peroxotungstic acid [WO₂(O₂)H₂O].

Preparation of WO₃ QDs

In the case of WO₃-QDs, we failed to obtain appropriate concentration of precursor solution (Not exceed 0.2M). Thus we modified our procedure to increase concentration of precursor species inside the pore.

Two grams of ground SMPS powder was dried overnight under a vacuum in a round flask to remove adsorbed water. The flask was then closed to maintain the reduced pressure. A WO₃ precursor solution equal to pore volume of SMPS (0.64, 0.59, and 0.32 cm³ for C6-W, C4-W, and C4V-W, respectively) was injected with a micro-syringe under reduced pressure. The wet powder was mixed vigorously for 1 h to ensure that the entire solution was confined in the pores. The sample was again dried under a vacuum for 3 h. This injection was repeated 2 to 3 times. The obtained dried powder was calcined in air at 673 K for 2 h.

ESR spin trapping experiment

A 40 mM DMPO ethanol solution was freshly prepared before usage. WO₃-confined SMPS or bulk WO₃ was added to the DMPO solution and dispersed by weak ultra-sonication. The bulk WO₃ was prepared by calcinations of the H₂WO₄ at 873 K for 3 h. The particle concentration was set to 40 mg/mL and 4.0 mg/mL for C4-W and bulk WO₃, respectively, to keep the ideal weight of WO₃ constant. Each suspension was introduced in an ESR flat cell and placed horizontally during the UV irradiation to prevent sedimentation of the particles. The ESR spectra were measured before and after 90 min UV irradiation by 6 W black light as a light source.

Characterizations

The nitrogen adsorption-desorption isotherms were obtained at 77 K with TriStar 3000 (Micromeritics) using samples pretreated under a vacuum at 433 K for 5 h. The specific surface area was calculated by the BET method. The pore size distribution was calculated by the BJH and GCMC methods. For the Grand Canonical Monte Carlo (GCMC) method, the BELSORP-max system (Nihon BEL, Inc.) was used for recording the isotherm, and BEL-Master software for was used for analyses. The analytical models of GCMC methods were as follows: pore models, oxygen-exposed surface with a cylindrical pore structure; adsorbate, nitrogen; peak assumption, Gaussian model with a single peak. The small angle X-ray diffraction patterns were recorded on a D8 ADVANCE (Bulker) with Cu K α radiation. Transmission electron microscopy (TEM) images were obtained using a TECNAI F20 (Philips) and Titan³ G2 60-300 (FEI). Diffuse reflectance ultraviolet-visible absorption spectra (DR-UV-Vis) were measured using a V-550 (JASCO) spectrometer equipped with an integral sphere. Electron spin resonance (ESR) spectra were measured using a Bulker E-500 spectrometer. ESR detection was performed by X-band spectrometry at the following settings: modulation frequency, 100 kHz; modulation amplitude, 5.00 G; receiver gain, 60 dB; time constant, 0.32 msec; conversion time, 81.92 msec; sweep time, 83.89 sec; center field, 3516.9 G; sweep width, 100.0 G; microwave power, 11 dB (15 mW); microwave frequency, 9.24 GHz. The intensity of each spectrum was calibrated using an ethanol solution of a TEMPO-free radical in a known concentration. The X-ray Photoelectron Spectrum (XPS) was measured using a PHI Quantera II (ULVAC Φ), without pre-sputtering. The

charge compensation of binding energy was done by using C1s peak position of surface contaminated carbon and confirmed by Si2p peak of SMPS.